

Adaptive semi-empirical model for non-contact atomic force microscopy

Xi Chen(陈曦), Jun-Kai Tong(童君开), and Zhi-Xin Hu(胡智鑫)

Citation: Chin. Phys. B, 2022, 31 (**8**): 088202. DOI: 10.1088/1674-1056/ac6eec
Journal homepage: http://cpb.iphy.ac.cn; http://iopscience.iop.org/cpb

What follows is a list of articles you may be interested in

Theoretical study on the mechanism for the excited-state double proton transfer process of an asymmetric Schiff base ligand

Zhengran Wang(王正然), Qiao Zhou(周悄), Bifa Cao(曹必发), Bo Li(栗博), Lixia Zhu(朱丽霞), Xinglei Zhang(张星蕾), Hang Yin(尹航), and Ying Shi(石英)

Chin. Phys. B, 2022, 31 (**4**): 048202. DOI: 10.1088/1674-1056/ac21c2

Substrate tuned reconstructed polymerization of naphthalocyanine on Ag(110)

Qi Zheng(郑琦), Li Huang(黄立), Deliang Bao(包德亮), Rongting Wu(武荣庭), Yan Li(李彦), Xiao Lin(林晓), Shixuan Du(杜世萱), and Hong-Jun Gao(高鸿钧)

Chin. Phys. B, 2022, 31 (**1**): 018202. DOI: 10.1088/1674-1056/ac3500

Equilibrium folding and unfolding dynamics to reveal detailed free energy landscape of src SH3 protein by magnetic tweezers

Huanhuan Su(苏环环), Hao Sun(孙皓), Haiyan Hong(洪海燕), Zilong Guo(郭子龙), Ping Yu(余平), and Hu Chen(陈虎)

Chin. Phys. B, 2021, 30 (**7**): 078201. DOI: 10.1088/1674-1056/abfb56

Influence of fluoroethylene carbonate on the solid electrolyte interphase of silicon anode for Li-ion batteries: A scanning force spectroscopy study

Jieyun Zheng(郑杰允), Jialiang Liu(刘家亮), Suijun Wang(王绥军), Fei Luo(罗飞), Liubin Ben(贲留斌), Hong Li(李泓)

Chin. Phys. B, 2020, 29 (**4**): 048203. DOI: 10.1088/1674-1056/ab7b54

Effects of rapid thermal annealing on room temperature NO_2-sensing properties of WO_3 thin film under LED radiation

Hu Ming, Jia Ding-Li, Liu Qing-Lin, Li Ming-Da, Sun Peng

Chin. Phys. B, 2013, 22 (**6**): 068204. DOI: 10.1088/1674-1056/22/6/068204

Adaptive semi-empirical model for non-contact atomic force microscopy

Xi Chen(陈曦)[1,†], Jun-Kai Tong(童君开)[1,2,†], and Zhi-Xin Hu(胡智鑫)[1,‡]

[1] *Center for Joint Quantum Studies and Department of Physics, Institute of Science, Tianjin University, Tianjin* 300350, *China*
[2] *State Key Laboratory of Precision Measuring Technology and Instruments, Tianjin University, Tianjin* 300072, *China*

(Received 7 April 2022; revised manuscript received 9 May 2022; accepted manuscript online 12 May 2022)

Non-contact atomic force microscope is a powerful tool to investigate the surface topography with atomic resolution. Here we propose a new approach to estimate the interaction between its tips and samples, which combines a semi-empirical model with density functional theory (DFT) calculations. The generated frequency shift images are consistent with the experiment for mapping organic molecules using CuCO, Cu, CuCl, and CuO_x tips. This approach achieves accuracy close to DFT calculation with much lower computational cost.

Keywords: semi-empirical model, atomic force microscopy, density functional theory, functionalized tips

PACS: 82.20.Wt, 68.37.Ps, 68.43.Fg, 71.15.Mb **DOI:** 10.1088/1674-1056/ac6eec

1. Introduction

The invention of atomic force microscopy (AFM) opened a new way to detect the surface geometry of solids.[1] The sub-molecular resolution of organic molecules was achieved by using CO-functionalized tip and qPlus technique.[2,3] The high performance of topography imaging enables its application in atomic recognition,[4,5] surface manipulation,[6,7] bond order recognition,[8–10] self-assembly,[11] and tracing reactions on surfaces.[12] The terminating CO molecule is chemically inert, which reduces the manipulation or bonding with the sample molecule. As the CO molecule is weakly attached to the tip apex, it could be deflected laterally when approaching the sample. The deflection of tip termination causes the distorted image for organic molecules, such as the shifted C–C bond length for the top ring of C_{60} molecule,[13] the enlargement of fluorinated carbon ring,[14] and the asymmetric image for a CO molecule.[15] The tip of non-contact AFM (nc-AFM) can also be functionalized by picking up Cl, Br, Xe or O atoms,[16–19] in which the chemical reactivity and the structural stability of the tip apex is responsible for the performance of imaging.

Theoretical simulations are needed to explain the contrast mechanism of nc-AFM. The interaction between tip and sample contains the short-range Pauli repulsion and the long-range attractions including electrostatic and van der Waals (vdW) forces. The former is responsible for the sub-molecular resolution while the later is dominant in the cases with long or medium tip-sample distances.[20–22] Density functional theory calculation is reliable to estimate the force between tip and sample, but the computational cost is not affordable for reproducing a high-resolution image. In order to reduce the cost, Moll *et al*. proposed a simple model in which a power law relation is assumed between the Pauli repulsion and the sample charge density.[23] The model works well for repulsive tip apex such as CO-functionalized tips, but the tip bending and attractive forces are absent. Hapala *et al*. introduced tip relaxation to the simulation and successfully reproduced the sharp sub-molecular contrast in nc-AFM observation.[24] Another way to accelerate the simulation is adding approximations to the DFT calculation, which could be achieved by implement of pseudopotential[25,26] or an efficient approach called frozen density embedding theories.[27,28] There are also methods that can simulate AFM images, such as Fourier expansion,[29] higher harmonic methods,[30] virtual tip methods,[31] and the method that can only be applied with graphene and graphite characterization.[32] The previous methods give results qualitatively similar to the experiment with affordable computational effort. The estimated tip-sample interaction still quantitatively differs from full DFT calculations.

In the present work, we develop an approach called force assisted simulation tool for atomic force microscopy (FAST-AFM) that combines a semi-empirical model with DFT calculation. The estimated tip-sample interaction forces are quantitatively comparable to DFT calculation, but the cost is much lower. This tool is applied to simulate the nc-AFM images of pentacene molecule on Cu(111) with CuCO, Cu, CuCl and CuO_x tips. The tool shows robust performance for all considered tips. It also achieves clear element identification while simulating the image of 4-bromo-3″-iodo-p-terphenyl (BrITP) molecule on Cu(111) and dicoronylene (DCLN) molecule on Cu(110).

[†]These authors contributed equally to this work.
[‡]Corresponding author. E-mail: zhixin.hu@tju.edu.cn

© 2022 Chinese Physical Society and IOP Publishing Ltd

2. Model and method of calculation

2.1. Formulation of the FAST-AFM

The force between tip and sample is contributed by different types of interaction, such as Pauli repulsion, coulomb interaction, bonding effect, van der Waals interactions. To make the model simple, we divide the force into the repulsive part and attractive part. The repulsive part is described with a modified Moll model, while the attractive part is proportional to the power of tip-sample distance. The Moll model uses the double atom system to describe the Pauli repulsion between tip and sample.[23] The kinetic energy decreases almost exponentially with tip-sample distances. The increase of kinetic energy is approximated to a simple model with two parameters and the sample charge density $\Delta E_{\rm kin}(R) = A\rho_{\rm s}(R)^B$. The Pauli repulsion energy is given by the increase of kinetic energy,

$$E_{\rm rep}(Z) = \frac{1}{Z}\int_Z^\infty A\rho_{\rm s}(Z')^B {\rm d}Z', \tag{1}$$

where Z is the tip-sample distance, $\rho_{\rm s}$ is the charge density of the sample, A and B are fitting parameters. The Pauli repulsive force is therefore the first derivative of the energy.

$$F_{\rm rep}(Z) = -\frac{\partial E_{\rm rep}(Z)}{\partial Z} = \frac{A}{Z^2}\int_Z^\infty \rho_{\rm s}^B(Z'){\rm d}Z' + \frac{1}{Z}\rho_{\rm s}^B(Z). \tag{2}$$

The Moll model has great performance for systems in which the Pauli repulsion is dominated, such as the AFM image for a PTCDA molecule with a CO functionalized tip.[23] However, due to the absence of the attractive interaction, the prediction may be poor for systems involving stronger attractive interaction. Attractive forces between tip and sample include electrostatic and vdW interactions etc. These forces are mostly proportional to $1/Z^N$ and related to the charge distribution. It is hard to induce dipole for highly localized electrons, which is expected to generate weaker vdW interactions. We define a modified localized electron function with the form of $|\frac{1}{\rho_{\rm s}}\frac{\partial\rho_{\rm s}}{\partial Z}|^M$ to rescale the strength of attractions. The attraction term is expressed as

$$F_{\rm att}(Z) = -C\left|\frac{1}{\rho_{\rm s}}\frac{\partial\rho_{\rm s}}{\partial Z}\right|^M \frac{1}{Z^N}, \tag{3}$$

with C, M, and N being fitting parameters. The repulsive and attractive parts are summed to generate the total force between the tip and samples. The expression of $F_{\rm rep}$ contains the integral of charge density while typical DFT calculations use mesh grids to describe the charge density. One solution is to transform the integral to the summation of discrete points, which requires accurate reproduction of the charge density, especially for the vacuum space. Here we assume that the charge density of an isolated atom decays exponentially with the distance R. The charge density far above the sample can be approximated to the form

$$\rho_{\rm s}(Z) = i\cdot {\rm e}^{-jZ}, \tag{4}$$

in which fitting parameters i and j can be estimated from a less accurate charge density mesh. Combine Eqs. (2)–(4), the total force can be expressed as

$$F_{\rm tot} = Ai^B {\rm e}^{-jBZ}\left(\frac{1}{jBZ^2}+\frac{1}{Z}\right) - C\left|\frac{1}{\rho_{\rm s}}\frac{\partial\rho_{\rm s}}{\partial Z}\right|^M \frac{1}{Z^N}. \tag{5}$$

This equation uses uniform Z for all positions, but the substrate with adsorbates is not absolutely planer. Even the flat pentacene molecule is bent on the Cu (111) surface. The charge density could be used to represent the difference in heights of atoms. Here we implement a correction h for the distance Z. The parameter h is the height of a charge density iso-surface relative to the molecular plane. The final form of the total force with h is

$$\begin{aligned} F_{\rm tot} =\ & Ai^B {\rm e}^{-jBZ}\left(\frac{1}{jB[Z'-h]^2}+\frac{1}{Z'-h}\right) \\ & - C\left|\frac{1}{\rho_{\rm s}}\frac{\partial\rho_{\rm s}}{\partial Z}\right|^M \frac{1}{Z^N}, \end{aligned} \tag{6}$$

where Z' shifts the height that makes $Z'-h$ equal to the tip-molecule distance in the molecular region. The implementation of h is essential to better reproduce the force, the necessity will be discussed in the next section.

The values for B and h are tested to get the best performance. It is found that setting B to 0.83 and the charge density iso-surface for h to 0.016 $e/{\rm \AA}^3$ is proper in the simulation. Other global parameters are optimized with the DFT calculated force curves.

The steps of simulation using this model are as follows:

(1) Get the sample charge density with DFT calculations. Build a tip model and calculate the force between tip and sample for several positions on the plane, which is used as the input force curve for the model.

(2) Functionalizing charge density using Eq. (4), get parameters i, j, h for each point.

(3) Fit Eq. (6) to the $F(Z)$ data acquired in step (1). Get global parameters A, C, M, and N.

(4) Build a mesh grid for the 2D contour of AFM simulation. Forces at each grid point can be calculated using Eq. (6).

We have programmed a toolbox to complete steps (2)–(4). What the user needs to do is running the initial DFT calculations and set a few tags. They are the charge density exponent B (can set to 0.83), the level of iso-surface ρ (can set to 0.016 $e/{\rm \AA}^3$), tip sample distance Z (can use multiple values if not sure), resonance frequency of the tip f_0 (according to the experiment set up), force constant in z direction, k_0, (from Hessian matrix or references), and the lateral force constant k (from Hessian matrix or references).

2.2. Density function theory calculations

The DFT simulations were performed with the Vienna *ab initio* simulation package (VASP) code with the Perdew–Burke–Ernzerhof (PBE) approximation for the exchange and correlation functional.[33] The dispersion correction was implemented using the DFT-D3 method.[34] Wavefunctions were described with a plane wave basis and the projector augmented wave method.[35] The cutoff energy for the plane wave basis was set as 400 eV. The first Brillouin zone was sampled by gamma point only for structural relaxation and force calculation, verified by a $2 \times 3 \times 1$ k-mesh. The charge density is calculated with the $2 \times 3 \times 1$ k-mesh for all systems, the $2 \times 3 \times 1$ mesh for the pentacene/Cu(111) system, and it is reduced to gamma-only sampling for DCLN and BrI-TP systems. For the sample system, a 4-layer slab model was built to simulate the substrate with a vacuum space of 35 Å. The size of the supercell is chosen to ensure 6 Å spacing between adsorbed molecules. The tip model was built with a tetrahedra cluster containing about 20 atoms. All atoms except for the bottom two layers of tip and substrate were fully relaxed until the residual force is less than 0.02 eV/Å per atom. Static calculations were performed to obtain the force curve. The charge density file is generated with the energy convergence set to 10^{-8} eV.

3. Results and discussion

The pentacene molecule adsorbed on the Cu (111) surface is a well-studied system in experiments. It contains the most common elements in organic molecules and various bonds such as σ and π bonds. Two sides of the molecule are slightly lifted up after the adsorption [Fig. S4(a)], making both sides slightly brighter than the middle in the AFM image. With this model, we first simulate the frequency shift image of the system and made a comparison with the experimental observation.

DFT calculations can produce a mesh grid of charge density. Figure 1(a) is the 2D map of sample charge density for the plane 3.2 Å above the molecule. The charge density plot has a dumbbell-shaped appearance due to the bending of the molecule. As mentioned in the method section, the charge density distribution is functionalized to an exponential form to ease the calculation. Some crucial positions such as C-top, C-hollow, H-top, and substrate were selected to judge the performance of the approximation, as shown in Fig. 1(b). It is clear that the exponential approximation fits the calculated charge density well for every curve. The detailed values of i and j are listed in Table S1.

The parameter h is introduced to consider the fluctuation of the sample surface. The pentacene/Cu(111) system is used again to run the test. Figure 2(a) shows the distribution of h with the iso-surface value $\rho = 0.016\ e/\text{Å}^3$. The tip-sample interaction forces are calculated for a 2×3 mesh with DFT. The tip is modeled by a tetrahedra-shaped Cu cluster with CO on the termination, as shown in Fig. 2(b). The fitted force curve for the model using Eq. (5) and (6) is shown in Fig. 3. The curves do not fit the DFT results well for points 4–6 without parameter h while the error is greatly reduced after adding h to the equation. This comparison proves the necessity of considering the surface fluctuation in the model.

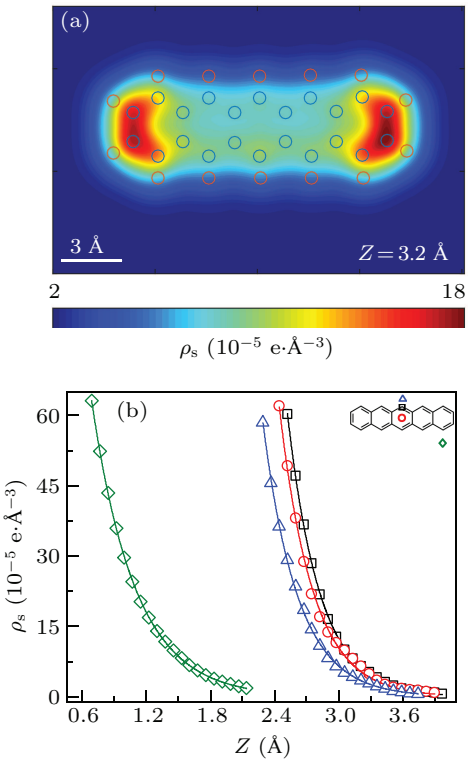


Fig. 1. Charge density for the pentacene molecule. (a) Two-dimensional map of the DFT calculated charge density above the pentacene molecule. The circles are the positions of atoms. (b) Charge density curves at crucial positions. The red circle, black square, blue triangle, and green diamond indicate the DFT results for C-top, C-hollow, H-top, and substrate, respectively. Solid lines are corresponding the functionalized values.

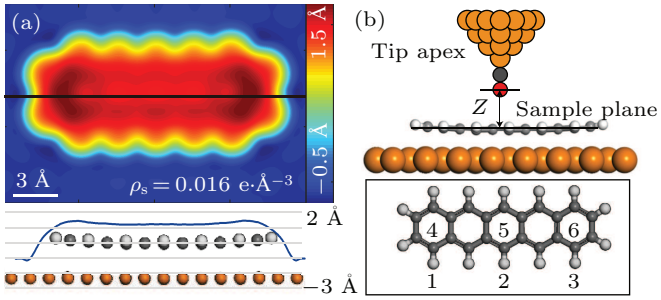


Fig. 2. The h profile and atomic structure of the tip-sample model. (a) Top- and side-view for the distribution of parameter h. The black line shows the cleaved slice of the side-view. (b) Atomic structure and the distribution for the 2×3 mesh used in the simulation. The orange, gray, red and white balls are copper, carbon, oxygen and hydrogen atoms, respectively. Points 1–3 of the mesh are away from the molecule while points 4–6 are within the molecular region.

The tip termination can be functionalized to get better performance in AFM observation. Pure metal tips made by Cu, Ag, and Au are too reactive for imaging organic molecules.[16,36] The tip apex becomes chemically inert by

attaching a CO molecule to the termination, which gives a better resolution of the atomic structure. However, the observed structure could be distorted as the terminating CO molecule is easily displaced by lateral forces.[13,14] Using halogen atoms to functionalize the tip can reduce the lateral distortion.[16] However, the resolution is worse than the CO-functionalized tip. Another good candidate for the functionalized tip is the oxidized copper tip. Harry *et al.* found that the CuO_x tip gives a clear backbone of aromatic molecules without distortion.[19,37] The diversity of tip terminations is a great challenge for AFM simulation. The FAST-AFM uses the DFT calculated force to optimize the parameters, which helps to adapt different tips.

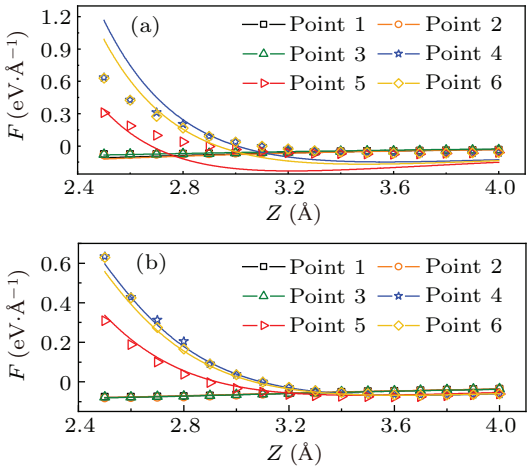


Fig. 3. DFT calculated forces (dots) and the simulated forces (curve) between CuCO tip and the pentacene/Cu(111). (a) Forces are simulated using Eq. (5). (b) Forces are simulated using Eq. (6). Black square, orange circle, green triangle, blue star, red triangle, and yellow rhombus indicates the 1-6 points, respectively.

First, we use FAST-AFM to reproduce the AFM image of pentacene/Cu(111) with the CuCO tip. The structural model and selected positions for DFT calculation are shown in Fig. 2(b). The optimized parameters are listed in Table 1. Figure 4 gives the simulated frequency shift image. The tip height is set as 3.8 Å to meet the range in the experiment. The simulated image shows clear carbon rings of the pentacene molecule. Two sides of the molecule are brighter than the middle due to the bending. The upper half of the middle ring is slightly darker than the lower half. The molecule is surrounded by a dark halo, which is thought to be caused by a diffuse attractive potential above the molecule.[16] As the CO molecule is loosely attached to the tip termination, it could be displaced laterally while probing the sample.[13–15] We modify the simulated image with a tip tilting correction, as shown in Fig. 4(c). The lateral force constant of the tip termination is set as $k = 0.5$ N/m.[8,24,38] Compared with the image without correction, the skeleton of the molecule becomes more sharp and bright elongation appears at C–H bonds. All of these features are consistent with the experimental observation shown in Fig. 4(b). These parameters in the equation are optimized using the DFT calculated forces for 2×3 mesh marked in Fig. 2(b). They are used without any further optimization to estimate force curves for crucial positions including C-top, C-hollow, H-top, and substrate. It is amazing that the estimated forces are almost identical to the DFT calculation. Relative errors are shown in Table S2. Values for the two terms on the right side of Eq. (6) are plotted in Fig. S1 in the Supplementary information. Both terms quickly decay with the distance. It needs to clarify that they are not equal to real repulsive or attractive forces, as the FAST-AFM is only a semi-empirical model with its parameters optimized by total forces from DFT calculation.

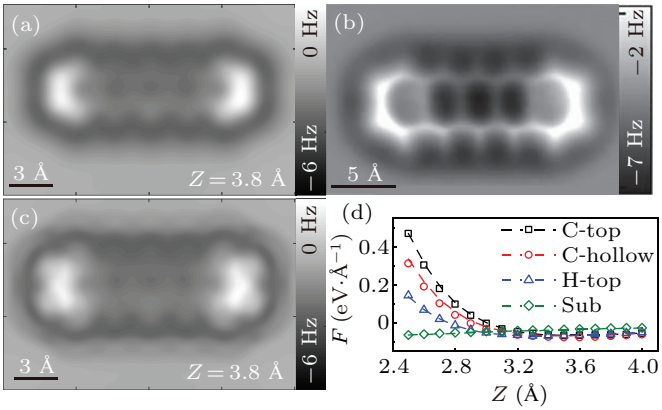


Fig. 4. FAST-AFM simulations for pentacene/Cu(111) with CuCO tip. (a) Simulated frequency shift image without tilting correction. Tip height is 3.8 Å. (b) Experimental image with CO-functionalized tip.[16] (c) Simulated frequency shift image with tilting correction at $Z = 3.8$ Å. (d) Simulated force curves (dashed lines) verses DFT calculations (dots) at crucial positions.

The FAST-AFM simulations were also applied to other tips including Cu, CuCl, and CuO_x. The frequency shift image for the Cu tip is calculated at a tip height of 5 Å, as shown in Fig. 5(a). Metal tips are too reactive to distinguish the inner structure of the pentacene molecule. The simulated image only gives a dark outline of the molecule, similar to the experimental observation using Ag tip (Fig. 5(b)). The reversed contrast of molecule and substrate indicates that the tip–sample interaction is attraction dominated. Successful reproduction of the attractive interaction is ascribed to the second term of Eq. (6), which is a reasonable supplement to the Moll model. For the CuCl tip, the 3p orbitals of the terminating Cl atom are almost filled after charge redistribution, making the CuCl tip less attractive than the pure Cu tip. The simulated AFM image in Fig. 5(c) is similar to that with the CuCO tip. The Cl atom is more tolerant to the lateral force due to strong Cu–Cl interaction. Less distortion is found in both the simulated image and the experimental image (Fig. 5(d)). The CuO_x tip is reported to have the submolecular resolution for organic molecules.[37,39]

Here we compare the simulated image to the AFM image of dicoronylene/Cu(110), as shown in Figs. 5(e) and 5(f). The adsorption structure of the DCLN/Cu(110) system and the sampling sites for force curves are shown in Fig. S2. The

DCLN is also an aromatic molecule with multiple carbon rings. The backbone of the molecule is bolder than the image produced by the CuCO tip. The negative frequency shift proves the attractive interaction between the CuO_x tip and the molecule. The simulated image reproduced the backbone of the molecule, while the brightness of the edge is different from the AFM image. The inconsisitence is ascribed to the optimized structure in which not all edge atoms are lifted up.

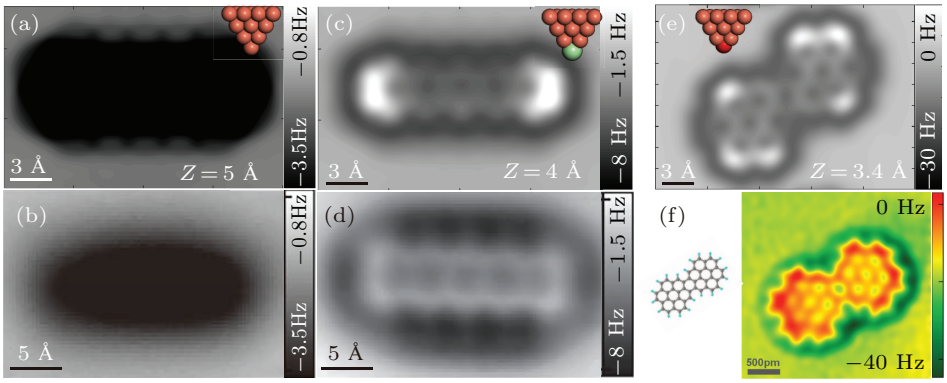


Fig. 5. FAST-AFM simulations with other tips. (a)–(d) Images of the pentacene molecule. (a) Simulated image for the Cu tip. (b) The nc-AFM image with Ag tip.[16] (c) Simulated image for the CuCl tip. (d) The nc-AFM image for pentacene/NaCl with CuCl tip.[16] (e) Simulated image for DCLN/Cu(110) with CuO_x tip. (f) The nc-AFM image for DCLN/Cu(110) with CuO_x tip.[37] The atomic models of corresponding tips are inserted to panels (a), (c) and (e).

The model is also applied to another molecule to test the performance for other elements. The nc-AFM images of the 4-bromo-3″-iodo-p-terphenyl (BrI-TP) molecule on the Cu(111) substrate are simulated using this model, as shown in Fig. 6. The CuCO tip is selected according to the experiment. The triphenyl group is slightly distorted due to the steric hindrance between H atoms, which leads to asymmetric brightness of benzene rings.[40] The Br atom is slightly higher than the I atom in the simulated image, while in the nc-AFM image they have almost identical brightness. This deviation is ascribed to the higher position of the Br atom in the relaxed structure of BrI-TP (Fig. S4(b)).

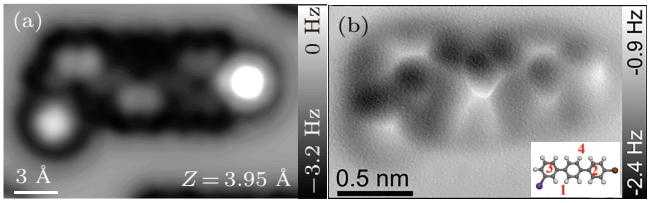


Fig. 6. FAST-AFM simulation and the experimental images for the BrI-TP/Cu(111) with CuCO tip. (a) Simulated image with $Z = 3.95$ Å. (b) Experimental image and the structure of BrI-TP molecule.[41] The purple, brown, gray, and white balls are I, Br, C, and H atoms, respectively. The 2×2 mesh is settled according to the shape of supercell.

The fitting parameters A, C, M and N for the previous simulation are listed in Table 1. A and C are scaling parameters for the repulsive and attractive terms, respectively. Larger value of A/C is related to a repulsive interaction between tip and sample. In our simulation the A/C values for CuCO tip, CuCl tip, and Cu tip are 48.28, 25.68, 20.09 respectively, showing a transition from repulsive dominating to attractive dominating. For pentacene, the CuO_x tip is abnormal with an A/C value of 16.59, showing a strong attractive regime. However, the imaging performance of the CuO_x tip is much better than the attractive Cu tip, the simulation image is shown in Fig. S5. The reason could be the high electronegativity of the oxygen atom, which creates a negatively charged termination and achieves the intramolecular resolution of the organic molecule.[37] The parameters M for all tips are around -3. This indicates that the effect of the modified localized electron function does not vary much with the choice of tips. The last parameter N decides the decay of attractive forces with the distance. A smaller value of N means that the attractive force is close to electrostatic interaction, while larger values mean that the attraction is mainly contributed by other vdW interactions such as dipole interaction etc. The simulation for the BrI-TP molecule is also applied with the CuCO tip, which gives A/C value similar to the pentacene case. As the charge distribution of halogen atoms is different from carbon or hydrogen atoms, the optimized values of M and N deviate from those for pentacene.

Table 1. Parameters obtained for two molecules and different tips using Eq. (6).

System	Pentacene				BrI-TP
Tip	CuCO	Cu	CuCl	CuO_x	CuCO
A	1461	4182	4975	1817	1829
C	30.26	208.18	193.72	109.51	27.67
M	–2.90	–3.19	–3.42	–3.52	–2.73
N	2.88	3.35	3.22	2.55	2.94

In FAST-AFM the parameters are optimized using the DFT calculated force curves as they are thought to have good accuracy. It is also easy to determine tip positions in DFT calculation. The small standard deviations between our model and DFT calculated force curves proves that our model has the potential to achieve accuracy similar to DFT calculations. However, the DFT calculated results differ from experiment for many reasons. The simulated structures of tip terminations or the adsorbates are not identical to the real system. Tip

vibration is ignored in the DFT calculated force. The calculated force may be inaccurate according to the selection of exchange-correlation functional and other calculation tags. All of these problems could cause the difference between the simulated image and the experimental observation.

The FAST-AFM method avoids the direct calculation of massive data points in the 2D map with an *ab initio* approach. The cost of this method can be divided into the DFT calculation and the parameter optimization. In this work, it only needs to calculate six force curves with DFT. The simulated forces are very close to DFT calculation at positions away from the selected mesh, even if the number of sampling force curves is reduced to 3 (Fig. S3). Taking the simulation for pentacene/Cu(111) as an example, which contains 228 atoms. The DFT calculation is conducted with 80 cores. It needs about two hours to get the charge density and 22 hours to get six force curves (15 min for each energy point). Then the FAST-AFM generates the simulated image of 280×180 dots within several minutes. On the other hand, in a full DFT calculation at least three energy points are needed to estimate the frequency shift for each position. The estimated time would be $280 \times 180 \times 3 \times 15$ min ≈ 37800 hours. The cost could be even higher if the tip-sample distance is unknown.

4. Conclusions

We have developed the FAST-AFM method to simulate nc-AFM images for organic molecules with limited cost and accuracy comparable to DFT calculations. This method is based on a semi-empirical model which describes repulsive and attractive interactions with the sample charge density. The parameters (A, C, M, N) are optimized with force curves from DFT calculation. By testing it on the pentacene/Cu(111) system, we find that the simulated images are highly consistent with the experiment for different functionalized tips, including the repulsive CuCO tip, less repulsive CuCl and CuO_x tips, and even the attractive pure Cu tip. This simulation tool also shows good elemental identification for the imaging of the more complicated molecule BrI-TP. The high accuracy and wide-range adaption of FAST-AFM make it a reliable method to conduct nc-AFM simulations for various systems.

Acknowledgements

Project supported by the National Nature Science Foundation of China (Grant No. 11804247). VASP Calculations were performed at the High-Performance Computing Platform from Center for Joint Quantum Studies of Tianjin University.

References

[1] Binnig G, Quate, C F, Gi E L and Gerber C 1986 *Phys. Rev. Lett.* **56** 930
[2] Liu M X, Li S C, Zha Z Q and Qiu X H 2017 *Acta Phys.-Chim. Sin.* **33** 183 (in Chinese)
[3] Giessibl F J 2019 *Rev. Sci. Instrum.* **90** 011101
[4] Sugimoto Y, Pou P, Abe M, Jelinek P, Pérez R, Morita S and Custance Ó 2007 *Nature* **446** 64
[5] Setvín M, Mutombo P, Ondráček M, Majzik Z, Švec M, Cháb V, Ošt'ádal I, Sobotík P and Jelínek P 2012 *ACS Nano* **6** 6969
[6] Li Y, Zheng Q, Chang X, Huang L, Lin X, Cheng Z H and Gao H J 2021 *Acta Phys. Sin.* **70** 136802 (in Chinese)
[7] Pang F, Cao F, Lei L, Meng L, Ye S, Xing S, Guo J, Dong H, Hussain S, Gu S, Xu K, Li Y J, Sugawara Y, Ji W, Xu R and Cheng Z 2021 *J. Phys. Chem. C* **125** 8696
[8] Gross L, Mohn F, Moll N, Schuler B, Criado A, Guitián E, Peña D, Gourdon A and Meyer G 2012 *Science* **337** 1326
[9] Ellner M, Pou P and Pérez R 2019 *ACS Nano* **13** 786
[10] Fan D, Sakai Y and Chelikowsky J R 2019 *Nano Lett.* **19** 5562
[11] Pawlak R, Kawai S, Fremy S, Glatzel T and Meyer E 2011 *ACS Nano* **5** 6349
[12] Albrecht F, Pavliček N, Herranz-Lancho C, Ruben M and Repp J 2015 *J. Am. Chem. Soc.* **137** 7424
[13] Guo C S, van Hove M A, Ren X and Zhao Y 2015 *J. Phys. Chem. C* **119** 1483
[14] Moll N, Schuler B, Kawai S, Xu F, Peng L, Orita A, Otera J, Curioni A, Neu M, Repp J, Meyer G and Gross L 2014 *Nano Lett.* **14** 6127
[15] Weymouth A J, Hofmann T and Giessibl F J 2014 *Science* **343** 1120
[16] Gross L, Mohn F, Moll N, Liljeroth P and Meyer G 2009 *Science* **325** 1110
[17] Mohn F, Schuler B, Gross L and Meyer G 2013 *Appl. Phys. Lett.* **102** 073109
[18] Yesilpinar D, Schulze Lammers B, Timmer A, Hu Z, Ji W, Amirjalayer S, Fuchs H and Mönig H 2021 *Small* **17** 2101637
[19] Mönig H, Amirjalayer S, Timmer A, Hu Z, Liu L, Díaz Arado O, Cnudde M, Strassert C A, Ji W, Rohlfing M and Fuchs H 2018 *Nature Nanotechnol.* **13** 371
[20] Moll N, Gross L, Mohn F, Curioni A and Meyer G 2010 *New J. Phys.* **12** 096102
[21] van der Lit J, di Cicco F, Hapala P, Jelinek P and Swart I 2016 *Phys. Rev. Lett.* **116** 125020
[22] Ellner M, Pavliček N, Pou P, Schuler B, Moll N, Meyer G, Gross L and Peréz R 2016 *Nano Lett.* **16** 1974
[23] Moll N, Gross L, Mohn F, Curioni A and Meyer G 2012 *New J. Phys.* **14** 083023
[24] Hapala P, Kichin G, Wagner C, Tautz F S, Temirov R and Jelinek P 2014 *Phys. Rev. B* **90** 085421
[25] Kim M and Chelikowsky J R 2015 *Appl. Phys. Lett.* **107** 163109
[26] Zahl P and Zhang Y 2019 *Energy Fuels* **33** 4775
[27] Wesolowski T A, Shedge S and Zhou X 2015 *Chem. Rev.* **115** 5891
[28] Sakai Y, Lee A J and Chelikowsky J R 2016 *Nano Lett.* **16** 3242
[29] Sasaki N, Aizawa H and Tsukada M 2000 *Appl. Surf. Sci.* **157** 367
[30] Wright C A and Solares S D 2011 *Nano Lett.* **11** 5026
[31] Chan T L, Wang C Z, Ho K M and Chelikowsky J R 2009 *Phys. Rev. Lett.* **102** 176101
[32] Castanié F, Nony L, Gauthier S and Bouju X 2012 *Beilstein J. Nanotechnol.* **3** 301
[33] Kresse G and Furthmüller J 1996 *Phys. Rev. B* **54** 11169
[34] Grimme S, Antony J, Ehrlich S and Krieg H 2010 *J. Chem. Phys.* **132** 154104
[35] Blöchl P E 1994 *Phys. Rev. B* **50** 17953
[36] Gross L, Schuler B, Mohn F, Moll N, Pavliček N, Steurer W, Scivetti I, Kotsis K, Persson M and Meyer G 2014 *Phys. Rev. B* **90** 155455
[37] Mönig H, Hermoso D R, Arado O D, Todorović M, Timmer A, Schüer S, Langewisch G, Pérez R and Fuchs H 2016 *ACS Nano* **10** 1201
[38] Fan D, Sakai Y and Chelikowsky J R 2020 *Phys. Rev. Mater.* **4** 053802
[39] Timmer A, Möing H, Uphoff M, Arado O D, Amirjalayer S and Fuchs H 2018 *Nano Lett.* **18** 4123
[40] Leng C, You S, Si Y B, Qin H M, Liu J, Huang W Q and Li K Q 2021 *J. Phys. Chem. A* **125** 2905
[41] Ebeling D, Zhong Q, Schlöder T, Tschakert J, Henkel P, Ahles S, Chi L, Mollenhauer D, Wegner H A and Schirmeisen A 2019 *ACS Nano* **13** 324